Maximum-Likelihood Estimation of the Directional Distribution of 0.53-Hz Ocean Waves

L. R. WYATT, L. J. LEDGARD, AND C. W. ANDERSON

Sheffield Centre for Earth Observation Science, School of Mathematics and Statistics, University of Sheffield, Sheffield, United Kingdom

(Manuscript received 11 March 1996, in final form 30 October 1996)

ABSTRACT

The maximum-likelihood method is used to extract parameters of two-parameter models of the directional spreading of short wind waves from the power spectrum of high-frequency (HF) radar backscatter. The wind waves have a wavelength of half the radio wavelength that, for the data presented here, is at a frequency of 0.53 Hz. The parameters are short-wave direction, which at this frequency can be identified with wind direction, and the directional spread angle, the parameterization of which is model dependent. For the data presented here, the results suggest that the Donelan directional spreading model provides a better description of directional spreading than the $\cos^s$ model. The HF radar and wave buoy measurements are compared and show good agreement. Measurements are presented that show the temporal and spatial structure of the short-wave field responding to the passage of a frontal system.

1. Introduction

Directional measurements are now routinely made with directional wave buoys that measure the spectrum from about 0.03 to 0.58 Hz, the upper and lower limits depending on the particular make of buoy. Comparisons between different buoy systems (Allender et al. 1989) show that mean directions are usually measured well, albeit with some biases at the low- and high-frequency ends of the spectrum. Measurements of directional spread can, however, be rather different and are apparently much more sensitive to the measurement technique. The modeling of directional spreading is also an area of active research. Theories have been developed to describe the variation of spread with frequency as a function of wind speed and in response to wind direction changes but there remain many uncertainties (Komen et al. 1994).

Techniques for the measurement of the directional spectrum using high-frequency (HF) radar systems have been developed at Sheffield University over the last eight years. The potential of using these methods with the OSCR (Ocean Surface Current Radar) HF radar system are now being investigated. Some preliminary results can be found in Wyatt (1994) and Wyatt and Ledgard (1996). OSCR is a high-resolution, short-range HF radar system developed in the United Kingdom and operating at the upper end of the HF band where theory suggests there may be limitations in the methods in high sea states (Lipa and Barrick 1986; Wyatt 1995). During 1994/95, OSCR was deployed on the northeast coast of England and one of the aims was to validate the wave measurement method and identify limitations. Due to a number of logistic hardware and software problems, the dataset available for such an objective was limited. The work described in this paper was motivated by a desire to make maximum use of the available data.

Measurement of the directional spectrum requires good signal-to-noise in the second order part of the power spectrum of the backscattered signal. This power spectrum (called the Doppler spectrum) is characterized by two peaks, the first-order spectrum, surrounded by the second-order continuum, the shape of which depends on the ocean wave directional spectrum. The scattering mechanism is Bragg scattering (Barrick 1972a). The two first-order Bragg peaks are associated with backscatter from waves of half the radio wavelength moving directly toward, to give a peak at positive frequency, or away from, for the negative peak, the radar site. For most of the experiment the signal-to-noise was only sufficient to identify the first-order peaks over most of the region of coverage.

The first-order peaks in the power spectrum are given by Barrick's equation (Barrick 1972b)

$$\sigma_1(\omega) = 2^6 \pi k_0 \sum_{m=\pm 1} S(-2mk_0)\delta(\omega - \omega_b), \quad (1)$$

where k_0 is the radio wavenumber; $S(-mk_0)$ is the ocean wave directional spectrum at the Bragg-matched ocean wavenumber, $2k_0$, moving toward ($m = 1$) or away from

Corresponding author address: Dr. L. R. Wyatt, University of Sheffield, School of Mathematics and Statistics, Applied Mathematics Section, P.O. Box 597, Sheffield S10 2UN, United Kingdom.
E-mail: L.Wyatt@sheffield.ac.uk

($m = -1$) the radar; and ω_b is the frequency of the Bragg-matched ocean waves; that is, $\omega_b = [2gk_0\tanh(2k_0d)]^{1/2}$, where d is water depth. Equation (1) describes two impulse functions at frequencies $\pm\omega_b$. The integral of the equation with respect to ω provides an estimate of $S(-2mk_0)$. In practice, the peaks are spread over a finite frequency band by current turbulence, system and signal processing effects, and so an integral over this finite frequency band is required to estimate $S(-2mk_0)$. The band has been determined by identifying local minima around the two peaks and integrating, using Simpson's rule, between these minima. The minima are usually 10 dB or more lower than the first-order peaks. If they are less than 3 dB down, an indication of current variability or severe sidelobe problems, the data are not analyzed further.

The directional spectrum at wavenumber k can be written as the product $S(k) = S(k)D(k,\theta)$, where $\int_{-\pi}^{\pi} D(k,\theta) = 1$ (see Tucker 1991), $k = |k|$, and $\theta = \arg(k)$. The difference in amplitude of the two Bragg peak integrals is determined entirely by $D(k,\theta)$. The HF radar measurements of wind direction can therefore be inferred from this amplitude difference. This is done using either a model of the directional distribution, $D(k,\theta)$—for example, a $\cos^s[(\theta - \theta_w)/2]$ model is often used with $s=4$ and θ_w being the direction of maximum energy—or by developing a semiempirical relationship between wind direction and first-order Bragg ratio (Georges et al. 1993). The integral of the power spectrum under the peaks is denoted by σ_+ for the approaching peak and σ_- for the receding peak. Using the model, the Bragg ratio r is thus given by

$$r = \frac{\cos^4\left(\dfrac{\phi + \pi - \theta_w}{2}\right)}{\cos^4\left(\dfrac{\phi - \theta_w}{2}\right)},$$

where the ratio is measured as $r = \sigma_+/\sigma_-$ and ϕ is the radar beam direction. This can be solved for θ_w, which is interpreted as wind direction under the assumption that the first-order Bragg waves are wind driven. There are limits to this assumption in low winds or low radio frequencies (Wyatt et al. 1986) and probably in rapidly varying conditions. With a single radar measurement there is a directional ambiguity in this measurement, the estimated θ_w will be either clockwise or counterclockwise from the radar beam. The resolution of this ambiguity requires a second radar or other information. Reasonable agreement has been found between wind directions estimated using a dual-radar system and independent wind measurements (Wyatt 1988).

The OSCR HF radar system operates at 27 MHz. The ocean waves generating the first-order Bragg peaks therefore have a frequency of 0.53 Hz. Wind speeds would have to be very low indeed for such frequencies not to be wind driven. The data presented here are from the Holderness dataset. These data were collected over the period November 1994 to early March 1995 off the Humberside coast of northeastern England. The experiment was aimed at developing an understanding of the dynamics of sediment transport in this region, which is subject to very rapid coastal erosion. In addition, the dataset is contributing to the SCAWVEX (Surface Current and Wave Variability Experiment) project. Various measurement systems were deployed, in addition to the OSCR HF radar, to provide 3D current fields, wave measurements, and sediment concentrations. In this paper the only measurements of interest are those from the directional waverider at an offshore location (referred to as N3, see Fig. 1). A different HF radar configuration was used from mid-February until early March 1995, but wave buoy measurements were not available after the end of February.

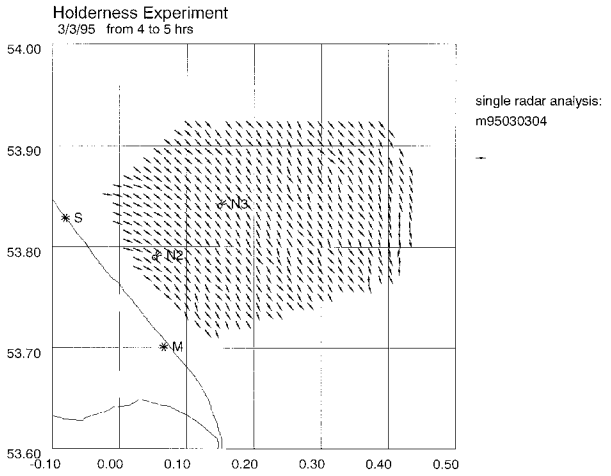

FIG. 1. Map showing location of the Holderness experiment and radar coverage during the second phase of the experiment. The two radar sites are shown: M—master site, S—slave site. The land shown in the lower left of the figure is the Humberside coast north of the Humber estuary, which is at the lower left-hand corner. One of two possible short-wave directions at each cell measured by the master radar shown with an arrow. The alternative directions are the reflection of those shown about the radar beam direction (the line from *M* to the point) at each point. The directional wave buoys at positions N2 and N3 are shown.

OSCR provides dual-backscatter measurements at up to 700 positions on a kilometer-scale grid with a range of up to 40 km. At each location the Bragg ratio can be measured and, using the model above, wind direction measured. A 5-dB limit on the minimum signal-to-noise is required before a measurement is made. Figure 1 shows an example of a typical configuration with wind directions measured using the southern radar system (known as the master for this deployment) shown at (nearly) all positions. Here one of the possible wind directions, that measured clockwise to the beam direction, has been selected arbitrarily. Wind directions estimated using the northern radar system (the slave) are shown in Fig. 2. This radar has a reduced range due to a power supply limitation. Figure 3 shows the same

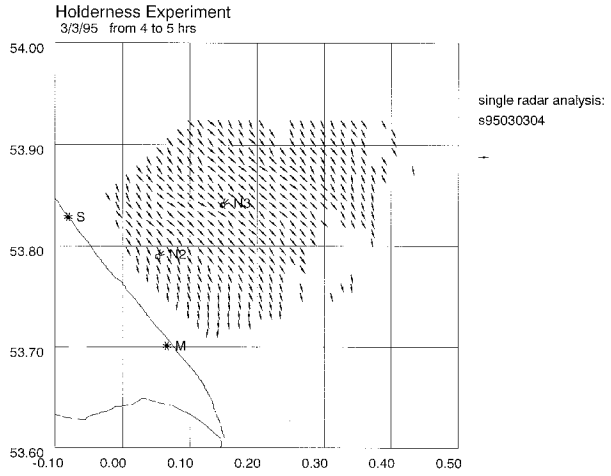

FIG. 2. As in Fig. 1 but for the slave site.

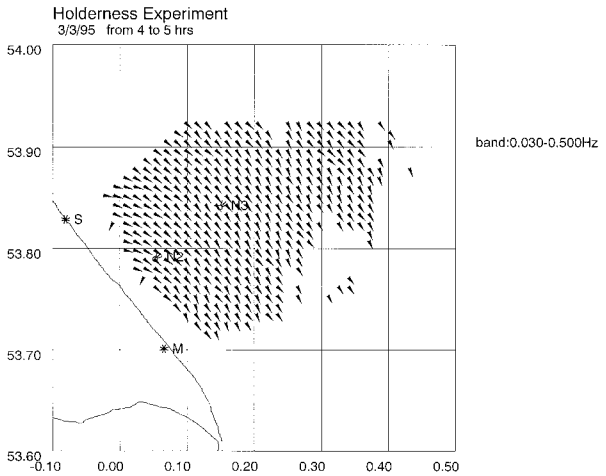

FIG. 3. Unambiguous dual-radar direction measurements.

wind field but with the ambiguity resolved by combining data from the two radar systems. The direction here is simply an average of the directions measured by the individual radars using the two (one from each) that are closer. Note that these two are not necessarily those shown in Figs. 1 and 2 where only one of two possible directions is plotted.

On examining the individual radar estimates carefully it is clear that in some locations and under some meteorological conditions there are significant differences between the single-radar direction estimates obtained using the above model. This is not so evident in the datasets presented in Figs. 1 and 2 although there are small differences at nearly all positions. These data were selected to demonstrate the validity of the new method that will be discussed below, and therefore a measurement of a fairly uniform wind field was used. Where differences do exist, when they are averaged out in the dual-radar estimates, increased variability in the wind direction field results. If one accepts that the two radars are indeed making the measurement at the same location, then these differences suggest that the model is not a good description of the directional spectrum at these frequencies. There is some evidence that antenna sidelobes do corrupt the first-order peaks in some circumstances, but this does not appear to be a major cause of the differences in wind direction estimates from the two radars except in a region close to the coast where the sidelobe problem is known to be most severe (Wyatt and Kingsley 1996). Two examples that could be attributable to this problem are seen at the western edge of the coverage region in Fig. 3. Other factors that could be responsible for the differences are a difference in signal-to-noise between the two measurements (although there is no consistent evidence for this in the data) and differences in the variances in the measurements.

The model that has been used is a one-parameter model with wind direction as the only variable. A two-parameter model has already been referred to: the $\cos^s[(\theta - \theta_w)/2]$ model where the parameter s is a measure of the directional spreading about the mean (wind) direction, θ_w. Other two-parameter models have also been suggested (Donelan 1985). In this paper a method for estimating the two parameters of a number of models is described. The aim of the method is to both estimate the parameters and to assess the best model for a given dataset. Heron (1987) also looked at the two-parameter estimation problem and derived estimates of θ_w and s, which were assumed to vary with range from the radar position but be constant with bearing so that two different beams separated by about 52° could be used in the analysis. The method described below provides a more general solution allowing variability in the parameters in both range and azimuth and taking into account the sampling variability in the measurements.

2. The method

The method adopted is that of maximum likelihood (Cox and Hinkley 1974). This method takes into account the statistical characteristics of the Bragg ratio measurement. Barrick (1980) and Sova (1995) have shown that the Bragg ratio varies according to an F distribution; that is, $r' \sim rF_{\nu,\nu}$, where r' is the measurement, r is the true Bragg ratio (which will be assumed to be the ratio obtained using the model in what follows), and $F_{\nu,\nu}$ is the F distribution with ν, the known degrees of freedom of the Doppler spectral estimates. The probability density function (pdf) of the F distribution is given by

$$\frac{\Gamma(\nu)F^{(\nu/2)-1}}{\left[\Gamma\left(\frac{\nu}{2}\right)\right]^2(1+F)^{\nu}}, \tag{2}$$

where F is the F distributed variable. Sova (1995) showed that the value of ν for the Doppler spectral estimates, which accounts for the windowing applied to

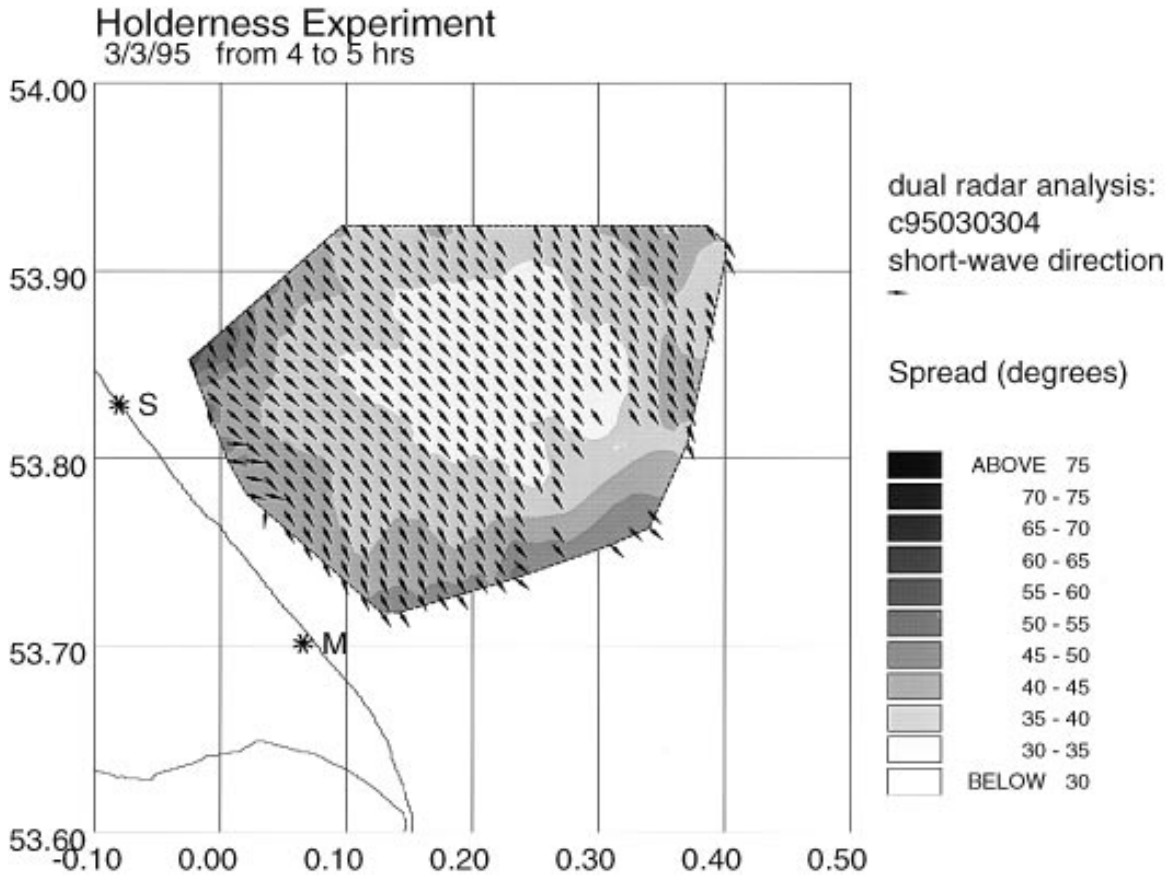

FIG. 4. Direction (arrows) and spread angle (gray scaled) for the cosine model.

the data, any overlapping of data segments and the averaging required to reduce the variance in the spectral estimates, is given (approximately) by

$$\frac{2}{\nu} = \frac{1}{M}[1 + 2\rho^2(75\%) + 2\rho^2(50\%) + 2\rho^2(25\%)] - \frac{2}{M^2}[\rho^2(75\%) + 2\rho^2(50\%) + 3\rho^2(25\%)] \quad (3)$$

(see also Harris 1978), where M is the number of data segments included in the average and $\rho(n\%)$ is the $n\%$ overlap correlation for the window used. OSCR data are available as 896 coherent I and Q measurements collected over 5 min. These are processed using four 512-point fast Fourier transforms after applying a Blackman-Harris four-sample window (Harris 1978) and overlapping by 75%. For this window the overlap correlations are given by

$$\rho(75\%) = 0.46,\ \rho(50\%) = 0.038,\ \rho(25\%) \approx 0.$$

Incoherent averages of three of these datasets are required to provide the variance reduction needed in the Doppler spectral estimate for wave measurement from the second-order Doppler spectrum. The degrees of freedom that result are three times that given by Eq. (2) and hence the value of $\nu = 18.2$ is used.

In the maximum-likelihood method we aim to maximize the likelihood of a set of observations with respect to the parameter set of a given model. Thus, we seek to maximize the expression $\Pi_{i=1}^{N}\text{pdf}(r'_i)$ or (more usually) $\Sigma_{n=1}^{N}\ln[\text{pdf}(r'_i)]$, where the subscript i denotes one of N measurements to be included, each of which has a different beam direction ϕ_i. Using Eq. (2), the pdf of the measured Bragg ratio $r' \sim rF_{\nu,\nu}$ is given by

$$\frac{\frac{1}{r}\Gamma(\nu)\left(\frac{r'}{r}\right)^{(\nu/2)-1}}{\left[\Gamma\left(\frac{\nu}{2}\right)\right]^2\left(1 + \frac{r'}{r}\right)^{\nu}}. \quad (4)$$

Thus, we are seeking to maximize

$$\sum_{i=1}^{N}\left\{\ln[\Gamma(\nu)] - 2\ln\left[\Gamma\left(\frac{\nu}{2}\right)\right] + \left(\frac{\nu}{2} - 1\right)\ln\left(\frac{r'_i}{r_i}\right) - \nu\ln\left(1 + \frac{r'_i}{r_i}\right) - \ln r_i\right\}, \quad (5)$$

where r_i denotes the model evaluated for measurement i, or equivalently minimize

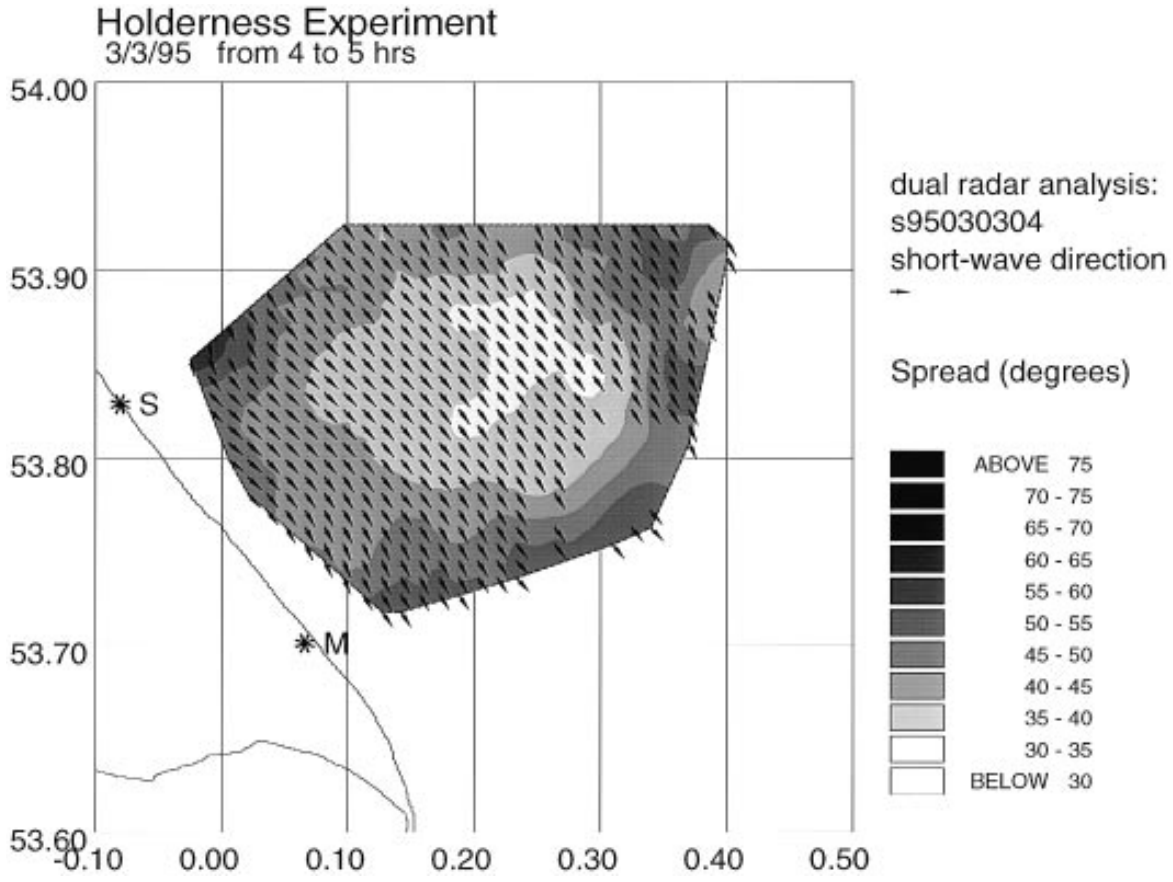

FIG. 5. As in Fig. 4 but for the Donelan model.

$$L = \sum_{i=1}^{N} \left\{ \nu \ln\left(1 + \frac{r_i'}{r_i}\right) - \left(\frac{\nu}{2} - 1\right)\ln\left(\frac{r_i'}{r_i}\right) - \ln[\Gamma(\nu)] + 2\ln\left[\Gamma\left(\frac{\nu}{2}\right)\right] + \ln r_i \right\}. \quad (6)$$

We are considering models for the Bragg ratio of the form $r_i(\theta_w, c, \phi_i)$, where θ_w is the mean direction and c is the model spreading parameter (e.g., s in the cosine model above) and ϕ_i is the radar beam direction for each measurement included in the minimization.

Clearly, if the measurements used are just those at a particular measurement cell from each radar, $N = 2$ and the problem can be solved exactly. Of course such an approach cannot answer the question ''Which model is best?,'' since exact solutions can be found in each case. Restricting the analysis to a single cell suggests that the spatial scale of homogeneity is expected to be of the order of 1 km^2. This is very fine spatial resolution for a wind field measurement. If we relax the requirements and assume homogeneity over a 10-km^2 region, then we can use data from the eight cells surrounding a particular cell giving $N = 18$ (since there are two looks at each cell) terms contributing to the minimization at that cell. This is the approach used here although, as will be seen, the results do still suggest kilometer-scale features in the wind field. Here N is, of course, reduced at the edges of the region and also where the quality of data in a particular cell is judged not to be sufficient for wind direction measurement, but the analysis is only carried out if $N \geq 4$. The use of more than one cell may also reduce the effect of antenna sidelobes, which are local in nature and unlikely to affect all the cells in the same way. Standard numerical library routines are used for the minimization with constraints imposed on the parameters; that is, the angle is constrained to the range 0–2π and the spreading parameter s, for the cosine model, ranges from 0 to 50. Different routines have been used, some of which make use of supplied functions $\partial L(\theta_w, c, \phi)/\partial\theta_w$, $\partial L(\theta_w, c, \phi)\partial c$, and also the second derivatives, as well as $L(\theta_w, c, \theta)$. All give similar answers although, for the cosine model at least, improvements in some regions are obtained if these explicit formulas for the derivatives are supplied. This seems to be because finite-difference estimates of the derivatives (which would otherwise be used) are not accurate when $\phi_i - \theta_w$ approaches 180°.

An example of a solution for θ_w and s [converted here into a spreading angle, σ, using $\sigma = [2(1 + s)^{-1}]^{1/2}(2\pi)^{-1}$ (Tucker 1991)] of the cosine model is shown in Fig. 4.

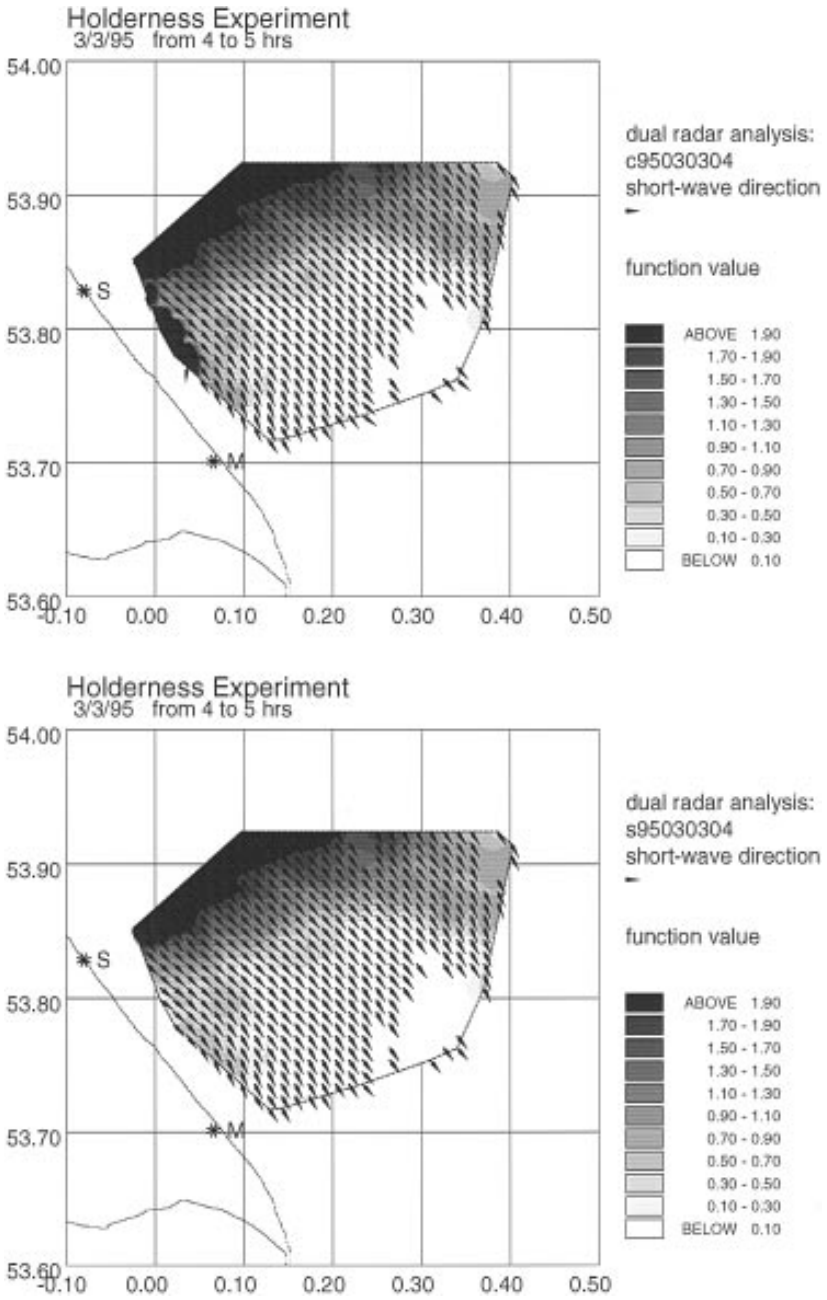

FIG. 6. Direction and minimum log likelihood (gray scaled) for the cosine model (a, upper) and the Donelan model (b, lower).

The wind field is similar to that shown in Fig. 3 but there are still regions that appear to be in error. These are west of the region where we expect sidelobe effects to be most adverse and where they are clearly evident within the spectral data at these points for this dataset. This is because the surface currents are large and fairly uniform across the region so radial current components in different directions are different and therefore sidelobe effects are separated in Doppler frequency. While the sidelobes will introduce errors at one or two cells, they do not do so in all cells, so their effect on parameter estimation is reduced. The apparent errors in direction estimates here are more likely to be associated with the fact that the ''true'' direction is near to the singularity in the model Bragg ratio, that is, when the waves are roughly aligned with the radar direction.

Other directional spreading models can be easily incorporated into the method. Figure 5 shows the results of applying the Donelan et al. (1985) model, $\mathrm{sech}^2\beta(\theta - \theta_w)$, where again the solution for β has been converted

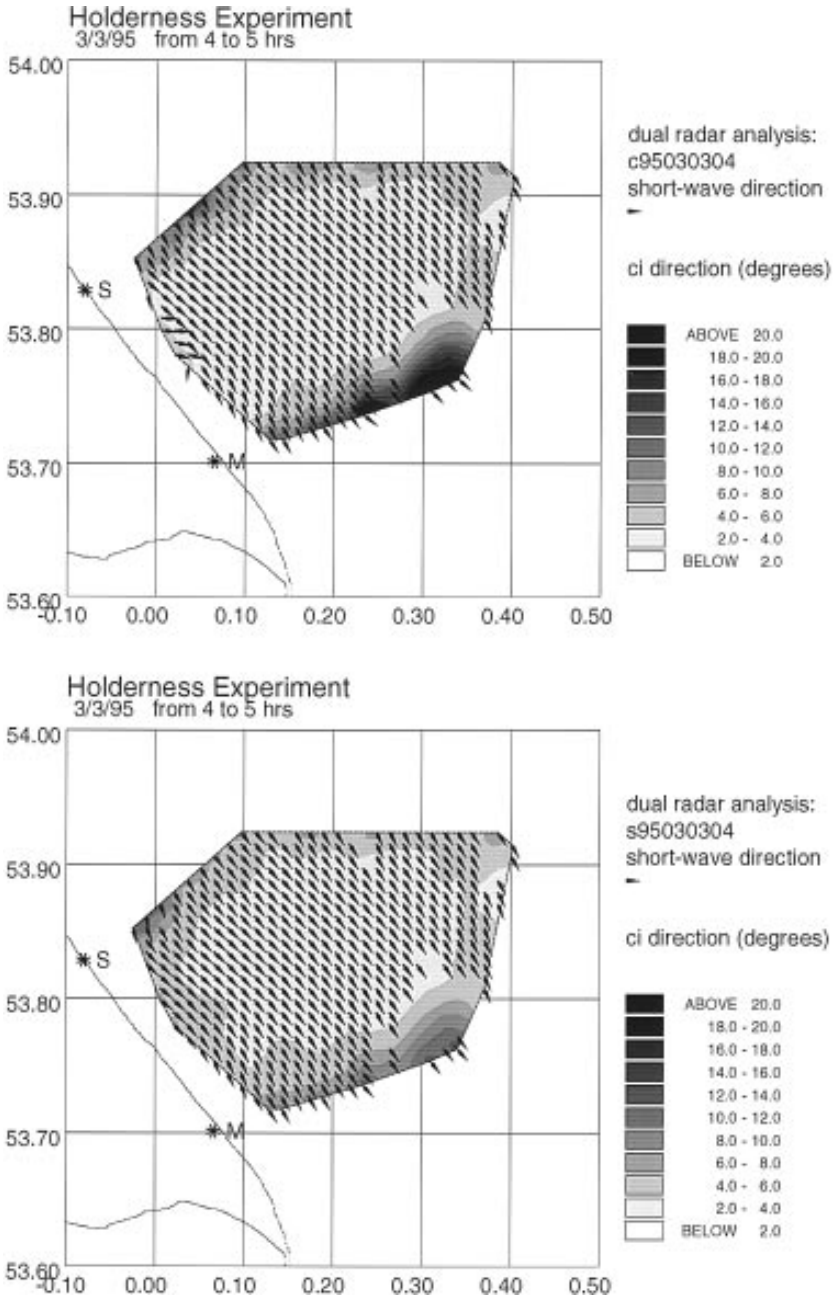

FIG. 7. Direction and confidence interval (gray scaled) for direction for the cosine model (a, upper) and the Donelan model (b, lower).

to a spreading angle for easier comparison with Fig. 4. The spreading angle was determined by evaluating the a_1, b_1 coefficients of the Fourier series expansion of $\text{sech}^2\beta(\theta - \theta_w)$ and using the formula used in the analysis of directional wave buoy data to determine σ, that is,

$$\sigma = \frac{\{2[1 - (a^2_1 + b^2_1)^{1/2}]\}^{1/2}}{2\pi}.$$

The range of values used for β was 0.1–3.0.

This model provides a more uniform wind field in the regions where the cosine model appeared to be in error. Figures 6a,b show a comparison of the quantity $L(\theta_w, c,\phi)/N$, where the division by N, the number of cells included in the analysis, is done so that cell to cell comparisons make sense. Over most of the region the two figures are very similar, but the cosine model in Fig. 6a shows larger values in the region already identified as a problem for this model. The values of $L(\theta_w, c,\phi)$ can be used to compare different models at one

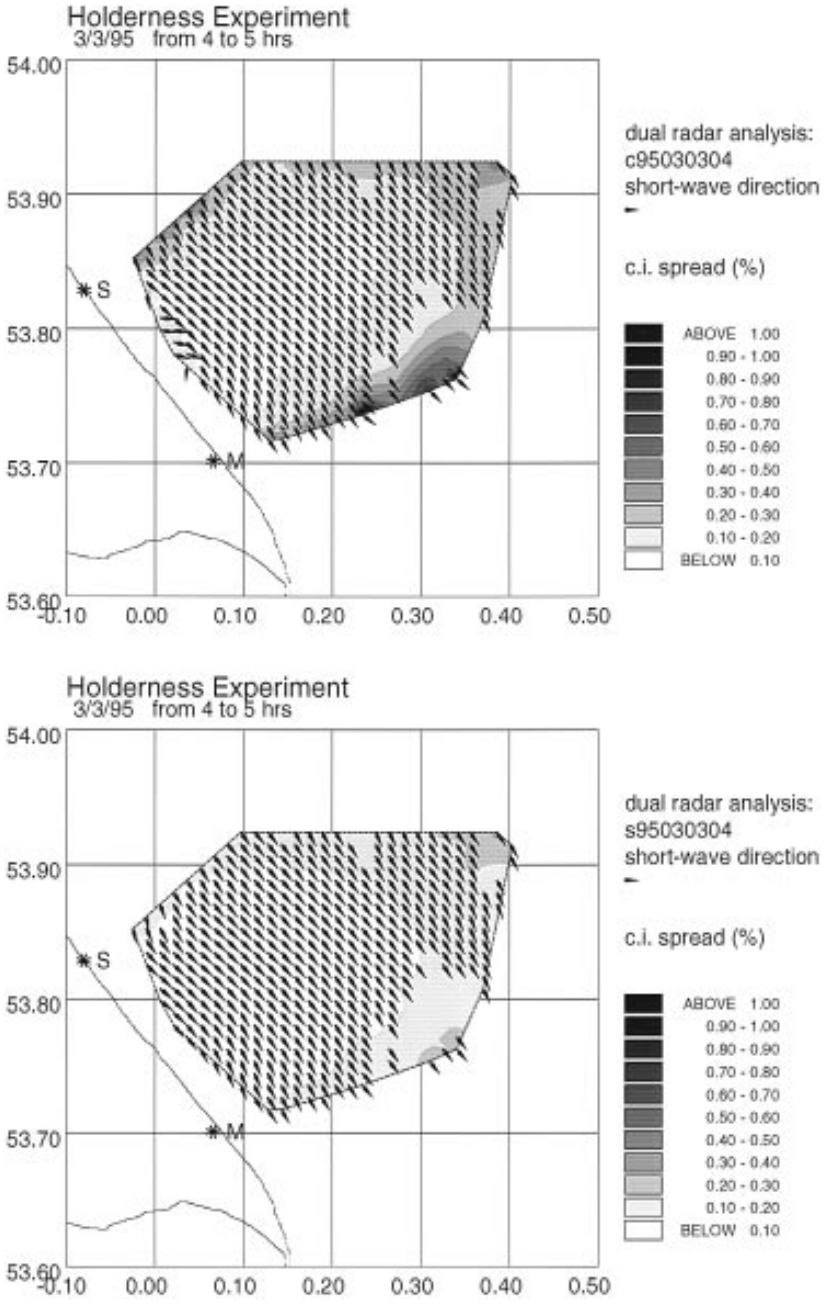

FIG. 8. Direction and confidence interval (gray scaled) for spread expressed as a proportion of the spread parameter for the cosine model (a, upper) and the Donelan model (b, lower).

location but cannot be used to indicate variations in accuracy for one particular model since the minimum reflects the angle of look at the short-wave field from each radar [through the $\ln r_i$ term in Eq. (6)]. In this example the waves are propagating toward the master radar in the north of the region giving a value of r_i greater than 1. In the south the waves are propagating away from the slave radar, giving a small value of r_i for that radar, and perpendicular to the master giving a maximum value for both radars of about 1 and thus a smaller minimum. In this second case, the minimum of L is approximately at the maximum of the F distribution, which is easily shown to be at $r'/r = (\nu - 2)(\nu + 2)^{-1}$, giving a value of $L/N \sim 0.065$ for the value of ν used here.

Confidence intervals (ci) for the parameter estimates can be calculated using the Hessian matrix

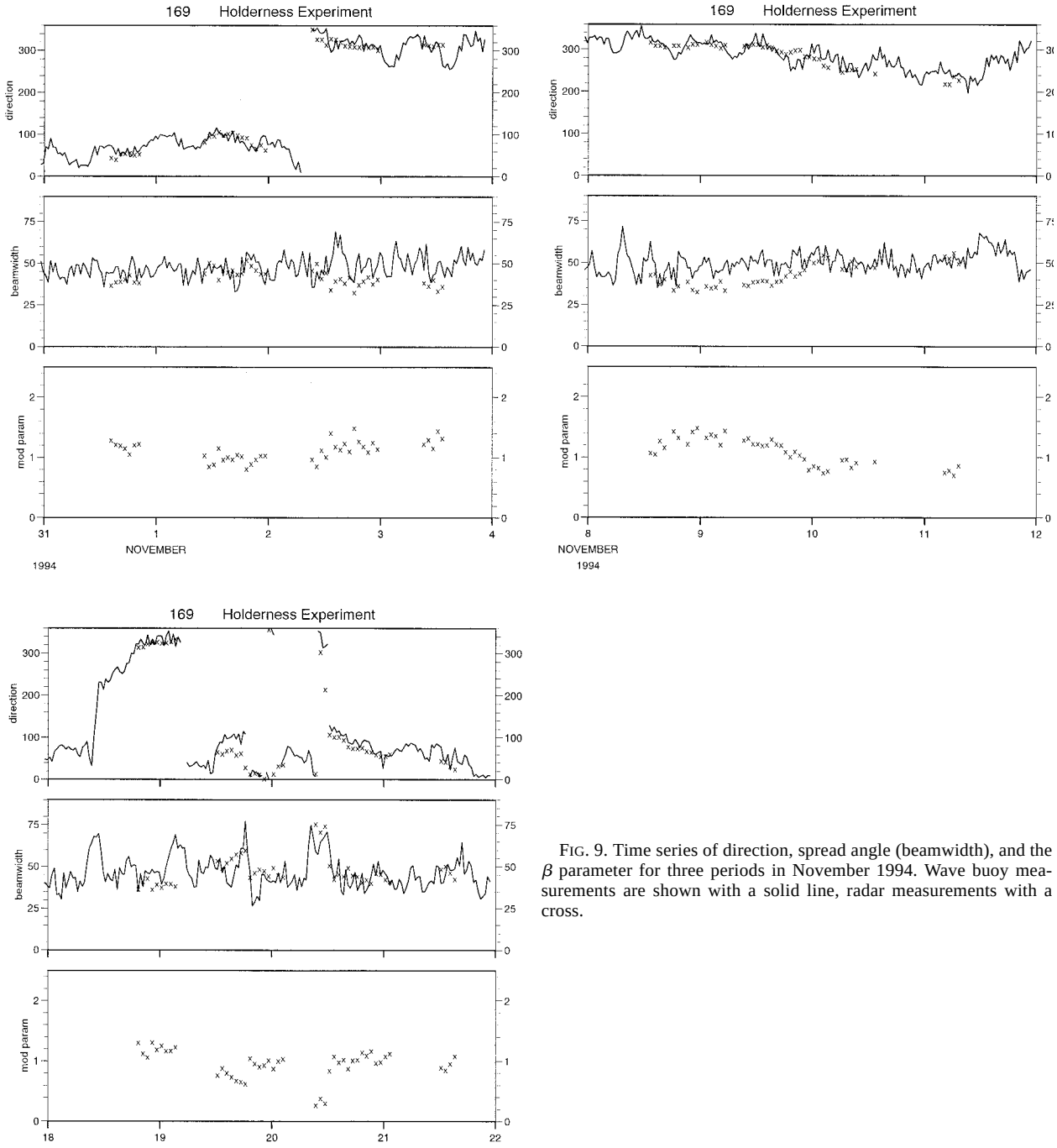

FIG. 9. Time series of direction, spread angle (beamwidth), and the β parameter for three periods in November 1994. Wave buoy measurements are shown with a solid line, radar measurements with a cross.

$$\mathbf{I} = \begin{bmatrix} \dfrac{\partial^2 L}{\partial \theta^2} & \dfrac{\partial^2 L}{\partial \theta \partial c} \\ \dfrac{\partial^2 L}{\partial \theta \partial c} & \dfrac{\partial^2 L}{\partial c^2} \end{bmatrix} \tag{7}$$

[using Eq. (6) for each model]. The confidence intervals are calculated from the inverse of this matrix so that the ci for θ is $\theta \pm 2\sqrt{\mathbf{I}^{-1}_{11}}$ and that for c is $c \pm 2\sqrt{\mathbf{I}^{-1}_{22}}$. All the second derivatives in the Hessian matrix were evaluated and coded into Fortran using Maple. Figures 7 and 8 show the confidence intervals for direction and the spread parameter (ci shown as a ratio of ci to the spread parameter), respectively, for the cosine (panel a) and Donelan (panel b) models. The cosine model has larger ci's in spread over most of the region and in

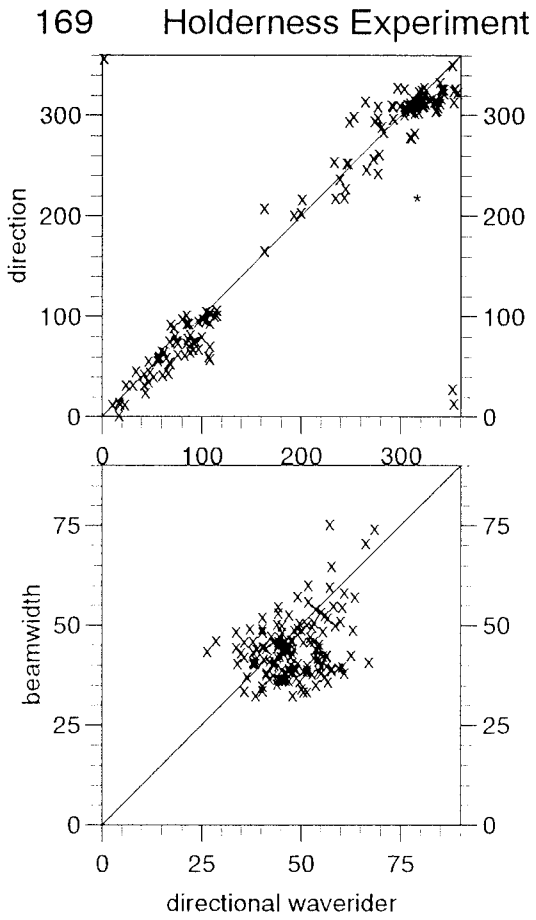

FIG. 10. Scatterplot of direction and spread angle, radar measurements on the *y* axis, wave buoy measurements on the *x* axis. The direction comparisons have a bias of −3.7° with a mean absolute difference of 14.7°; corresponding figures for spread are −3.7° and 7.8°.

direction at the edges of the region. Similar behavior was found with different datasets and so the Donelan model is used in the rest of this paper. The implication is that the Donelan model is providing a better description of the short-wave directional characteristics of this dataset. The larger ci's shown by both models at the edges of the region are likely to be related to reductions in signal-to-noise in at least one of the radars in these regions. Unlike *L*, confidence intervals can be used to look at the spatial variation in the precision of the measurements.

3. Application to Holderness data

OSCR wave measurements were not obtained continuously throughout the experiment due to on-site data storage limitations and to various hardware and software problems that interrupted operations. Figure 9 shows time series of θ_w and c (converted to a spreading angle) measured by the radar using the method described above at the N3 location and by the waverider (at 0.53 Hz) for three periods when OSCR was operating. The waverider measurements are of directional spreading defined using the a_1, b_1 Fourier coefficients determined directly from the data. The β parameter is also plotted for the radar data and shows that the value is less than the minimum of 1.24 in the Donelan model for most of this dataset. This minimum represents a mean of rather noisy measurements that were at a lower frequency than these OSCR and wave buoy measurements. This seems to suggest that the reduction in β with frequency in the Donelan model should be extended to higher frequencies. It should be borne in mind when judging the radar–wave buoy comparisons that the radar measurements are obtained using data averaged from three separate 5-min data collections (from each radar) over a 45-min period (Wyatt and Ledgard 1996), whereas the waverider measurements are for averages over a 20-min continuous data collection so some differences are expected. This is particularly true during periods of large wind direction change when, as will be shown below, timescales of change in the directional characteristics can be quite short. Scatterplots showing the comparisons for all OSCR data collected during the period are shown in Fig. 10. Direction comparisons are good, those of spread appear to be more scattered, although it should be borne in mind that wave buoy measurements show similar scatter in this parameter [Allender et al. (1989) although note that their analysis did not extend to the high frequency of these measurements] and the range of this measurement is small.

One interesting period seen in Fig. 9 is 20 November with a large change in direction and spread toward the middle of the day. Unfortunately there was a break in radar coverage during the morning so the initial development was not captured, but in the later stages of development and the relaxation to a steady wind direction, the radar and wave buoy measurements show very similar features. Figure 11 shows the time series of spatial development of the high-frequency wave directional characteristics during this period. There appears to be a front propagating roughly from northwest to southeast through the region with a lot of associated frontal wave activity on kilometer spatial scales. Directional spreading is seen to increase ahead of and within the frontal region and then decrease again as the wave field settles down behind the front. The changes seen here in the high-frequency wave direction, assumed to be closely aligned with the wind direction, are consistent with the movement through the region of a wavy front seen in Meteorological Office charts at 1200 UTC, although the spatial and temporal resolution in the radar data provides structural details that cannot be verified. Figure 12 shows the direction confidence intervals, and it is clear that these are large where the frontal activity is occurring and where the spreading is large. Not surprisingly there does appear to be a relationship between the spread angle and the direction confidence interval. This requires further study.

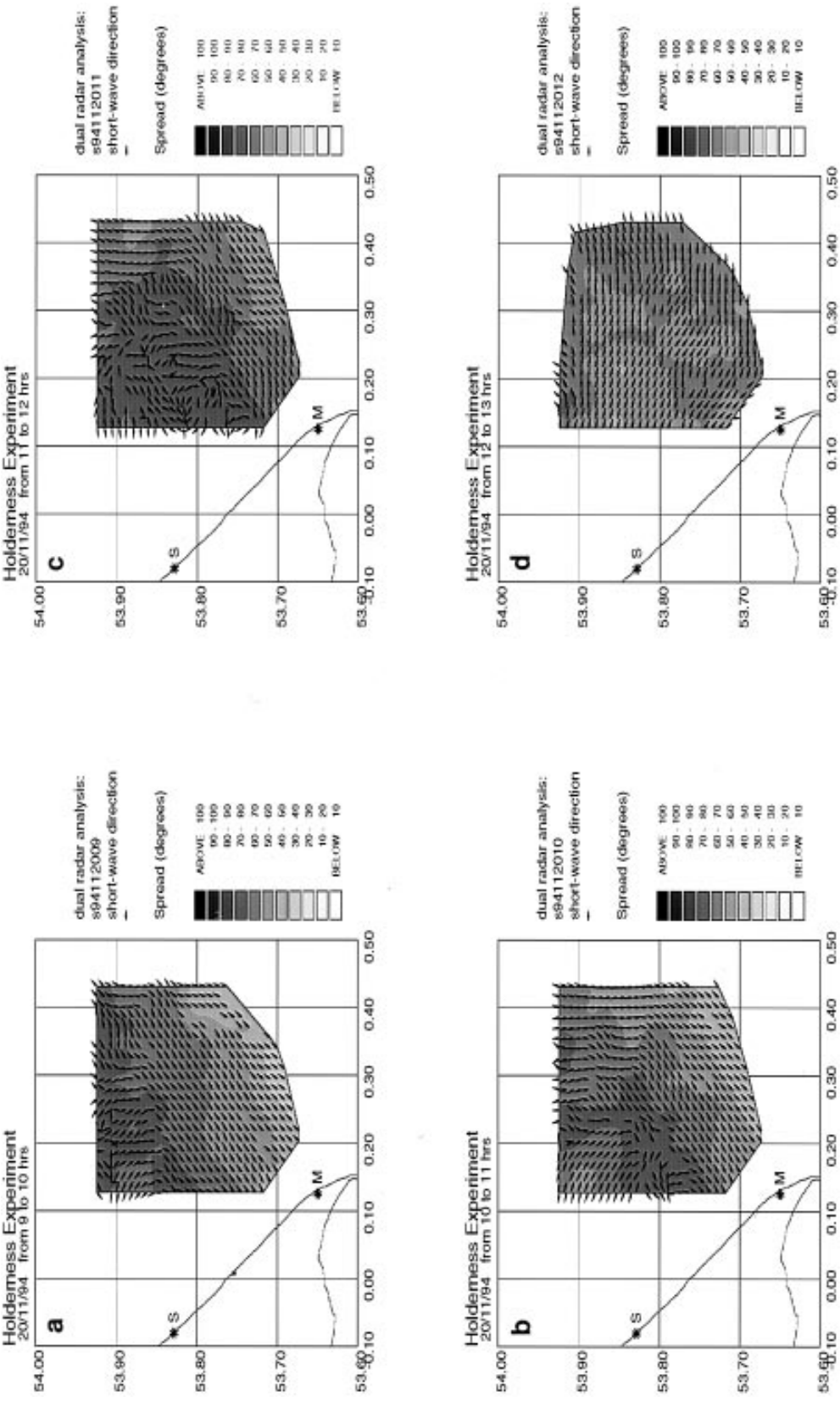

FIG. 11. The spatial and temporal variation in short-wave direction and spread (gray scaled) during the passage of a frontal system during the first phase of the experiment. Data were lost to the west of the region due to a beamforming error. Southwesterly winds in advance of the front (a) are replaced by northwesterly winds behind the front (d). Wave and eddy activity can be seen under the front.

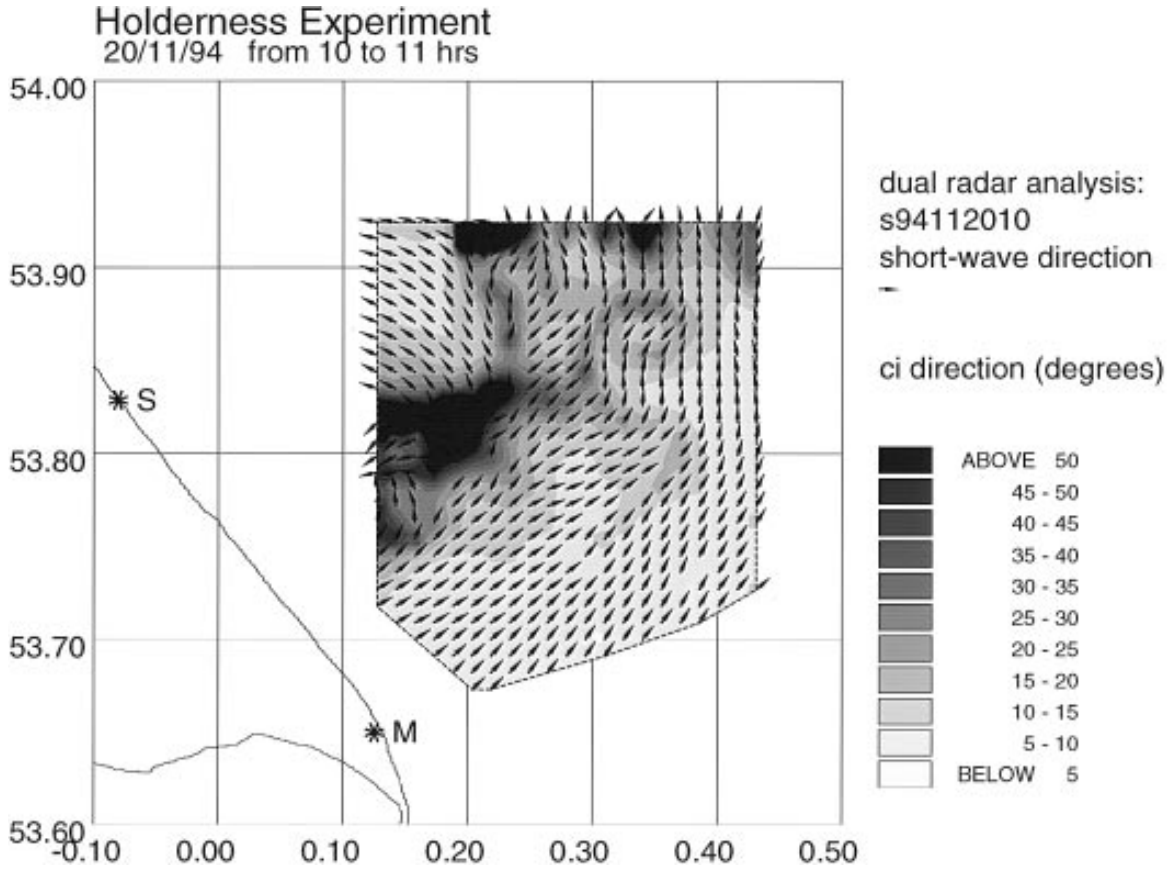

FIG. 12. Confidence intervals (gray scaled) showing increased direction confidence intervals under the front.

The complicated nature and rapid development of wave activity in response to the front suggests that the 45-min averaging used here is too long. This particular dataset has been reanalyzed to allow for 10-min averages during the period of intense frontal activity. This increases the variance in the estimates, but this is taken into account in the analysis. The results suggest that the detailed structure does indeed change on timescales of the order of 10 min. The measurements shown in Figs. 9–12 are therefore strictly only valid away from the region of short-timescale variability. Nonetheless the 45-min averages do give a good impression of the larger scale development. More work is needed to assess the validity of the spatial structure seen in these measurements.

The 45-min averages have been used in this work because these are required for measurement of the ocean wave directional spectrum through inversion and the data was analyzed with this aim in mind. Clearly such averaging is not appropriate for the spectral measurements either when stationarity does not apply. Other methods for reducing variance in the Doppler spectral estimates without using such long averaging times are under investigation. Ten-minute averages are in fact available as part of the normal operation of OSCR so that the method presented here could be applied directly to the data on site as an addition to the standard current measurement processing.

4. Concluding remarks

A new technique for measuring the directional spectrum of high-frequency ocean waves using HF radar has been presented here. Good agreement with wave buoy measurements of direction has been demonstrated. Directional spreading comparisons show some agreement but are less convincing, although whether this can be attributed, at least in part, to errors in the buoy measurement remains to be established. The method can be used with any two-parameter directional spreading model, and the models can be judged by looking at the minimum value of the negative log-likelihood and at the confidence intervals for the parameter measurements. These suggest that the Donelan et al. (1985) directional spreading model provides a better description than the more standard $\cos^s$ model of the wave fields observed at Holderness, although the value of the β parameter tends to be smaller, implying broader directional spreads. This may be associated with the nature of the wave fields that are often fetch limited over deepening waters or subject to changing wind directions or, as mentioned earlier, simply indicate the need to extend

the Donelan model to higher frequencies. Although a method for distinguishing between directional spreading models has been suggested and an application of this method to this particular dataset has provided some support for the Donelan model, further work is needed to confirm, or otherwise, this result, focused as far as possible on idealized conditions with unimodal wave fields.

The good spatial and temporal resolution available with HF measurements reveals interesting structure in the wave field in response to weather frontal systems. Such measurements will be of interest to those concerned with understanding boundary layer processes over the sea. In future experiments it may be possible to verify some of the observed spatial structure by making comparisons with wave data at different locations. Unfortunately, during the Holderness experiment the other directional wavebuoy was at a location where the radar data seems to be subject to antenna sidelobe problems (N2 in Fig. 1). Because data from more than one location are used in the fitting, errors due to sidelobes appear to be minimized using the method that has been presented here. Nonetheless, they will have some influence and should be avoided, if possible. More seriously, a beam-forming error during the first half of the experiment means that there is only a limited amount of dual-radar data that can be compared with this buoy and none during the event shown in Fig. 11. However, the good temporal agreement between the N3 buoy and the radar during this period of rapidly changing short-wave direction indicates that the spatial structure seen in the radar data is unlikely to be much in error.

Acknowledgments. This work was partly funded by the Ministry of Agriculture, Fisheries and Food under the Flood Protection Commission FD0306 with the Proudman Oceanographic Laboratory and NERC Contract F3CR07-G1-02. The OSCR system used was provided by NERC and deployed by the NERC OSCR unit at Southampton University. We are grateful to the anonymous reviewers for a number of useful suggestions on presentation and content.

REFERENCES

Allender, J., and Coauthors, 1989: The WADIC project; a comprehensive field evaluation of directional wave instrumentation. *Ocean Eng.,* **16,** 505–536.

Barrick, D. E., 1972a: Remote sensing of sea state by radar. *Remote Sensing of the Troposphere,* V. E. Derr, Ed., U.S. Government Printing Office, 12.1–12.6.

——, 1972b: First-order theory and analysis of MF/HF/VHF scatter from the sea. *IEEE Trans. Antennas Propag.,* **AP-20,** 2–10.

——, 1980: Accuracy of parameter extraction from sample-averaged sea-echo Doppler spectra. *IEEE Trans. Antennas Propag.,* **AP-28,** 1–11.

Cox, D. R., and D. V. Hinkley, 1974: *Theoretical Statistics*. Chapman Hall, 511 pp.

Donelan, M. A., J. Hamilton, and W. H. Hui, 1985: Directional spectra of wind-generated waves. *Philos. Trans. Roy. Soc. London, Ser. A;* **315,** 509–562.

Georges, T. M., J. A. Harlan, L. R. Meyer, and R. G. Peer, 1993: Tracking Hurricane Claudette with the U.S. Air Force over-the-horizon radar. *J. Atmos. Oceanic Technol.,* **10,** 441–451.

Harris, F. J., 1978: On the use of windows for harmonic analysis with the discrete Fourier transform. *Proc. IEEE,* **66,** 51–83.

Heron, M. L., 1987: Directional spreading of short wavelength fetch-limited wind waves. *J. Phys. Oceanogr.,* **17,** 281–285.

Komen, G. J., L. Cavaleri, M. Donelan, K. Hasselmann, S. Hasselmann, and P. A. E. M. Janssen, 1994: *Dynamics and Modelling of Ocean Waves.* Cambridge University Press, 532 pp.

Lipa, B. J., and D. E. Barrick, 1986: Extraction of sea state from HF radar sea echo: Mathematical theory and modelling. *Radio Sci.,* **21,** 81–100.

Sova, M. G., 1995: The sampling variability and the validation of high frequency radar measurements of the sea surface. Ph.D. thesis, University of Sheffield, 146 pp. [Available from L.R. Wyatt, School of Mathematics and Statistics, University of Sheffield, P.O. Box 597, Sheffield S10 2UN, United Kingdom.]

Tucker, M. J., 1991: *Waves in Ocean Engineering: Measurement, Analysis, Interpretation.* Ellis Horwood, 431 pp.

Wyatt, L. R., 1988: HF radar wind measurement during NURWEC2. *Proc. IGARSS ′88 Symp.,* Edinburgh, Scotland, European Space Agency, 781–782.

——, 1994: Coastal surface current and wave measurement with HF radar: Limitations and prospects. *Mixing and Transport in the Environment,* K. Beven, P. C. Chatwin, and J. H. Millbank, Eds., John Wiley and Sons, 295–306.

——, 1995: High order nonlinearities in HF radar backscatter from the ocean surface. *IEE Proc.: Radar, Sonar and Navigation,* **142,** 293–300.

——, and S. P. Kingsley, 1996: OSCR antenna beam measurement. Final Rep. to the Natural Environment Research Council, Grant GR9/02095, 9 pp. [Available from L.R. Wyatt, School of Mathematics and Statistics, University of Sheffield, P.O. Box 597, Sheffield S10 2UN, United Kingdom.]

——, and L. J. Ledgard, 1996: OSCR wave measurements: Some preliminary results. *IEEE J. Oceanic Eng.,* **21,** 64–76.

——, J. Venn, M. D. Moorhead, G. D. Burrows, A. M. Ponsford, and J. van Heteren, 1986: HF radar measurements of ocean wave parameters during NURWEC. *IEEE J. Oceanic Eng.,* **OE-11,** 219–234.